Inhibition of sodium release from Zhundong coal via the addition of mineral additives: a combination of online multi-point LIBS and offline experimental measurements

Yingzu Liu[1,3], Zhihua Wang[1], Yu Lv[2], Kaidi Wan[1,*], Yong He[1], Jun Xia[3], Kefa Cen[1]

1. State Key Laboratory of Clean Energy Utilization, Zhejiang University, Hangzhou 310027, China

2. Department of Mechanical Engineering, Stanford University, Stanford, CA 94305, USA

3. Department of Mechanical, Aerospace and Civil Engineering & Institute of Energy Futures, Brunel University London, Uxbridge UB8 3PH, UK

* Corresponding author: wankaidi@zju.edu.cn

Abstract

The retention performance of 5 different sorbent additives, including 2 pure additives, i.e., silica and alumina, and 3 typical natural mineral additives, i.e., kaolin, mica and pyrophyllite, on the release of sodium during the combustion of Zhundong coal is investigated via a combination of online multi-point Laser-Induced Breakdown Spectroscopy (LIBS) technique and offline measurements including inductively coupled plasma atomic emission spectrometer (ICP-AES), X-ray diffraction, and ash fusion temperatures (AFTs). The online and offline measurement results for the sodium release of Zhundong coal/additives mixtures are compared and verified with each other. Ternary phase diagram simulations are performed to further substantiate the impact of different additives on liquidus temperatures of Zhundong coal ash. All the five sorbent additives show a significant sodium retention effect, while alumina and kaolin are better additives considering the effects on AFTs.

Keywords: Zhundong coal; Sodium; Alkali metal; sorbent additives; LIBS

1. Introduction

Coal, as an energy source, supports approximately 40% of the worldwide electricity [1]. Due to its broad availability and the flexibility of coal combustion systems, the utilization of coal is expected to continue in the near and medium future [2, 3]. It was known that the presence of sodium in coal can lead to rapid ash deposition on heat transfer surfaces of coal-fired boilers [4]. By reacting with chloride and sulfur species in the gas phase, sodium can also form complex chloride and sulfur compounds, which leads to fouling and corrosion of heat transfer surfaces [5]. These sodium-induced issues significantly restrict the utilization of the low rank coal with a relatively high sodium concentration, e.g., Zhundong coal [6]. The new 390-billion-ton Zhundong coalmine has been recently explored in China. Under the current consumption rate of coal, this new source of coal supply is able to support the energy demand of China for more than 100 years [7]. However, utilization of this new source of Zhundong coal requires reducing the harmful sodium emissions during coal combustion [8].

Better understanding of the release characteristics of sodium plays a key role in the development of these sodium-controlling technologies. In the past decades, research on sodium release during coal combustion mainly employs offline measuring techniques, e.g., sampling measurements by analyzing the bulk composition of fly ash and ash deposits [9]. According to the pioneering work in the field, the forms of sodium in coal can be categorized to four classes [10, 11]: (1) water-soluble sodium, which can be dissolved within moisture and exist as Na salts; (2) NH_4Ac-soluble sodium, which is organically bounded with carboxyl groups; (3) HCl-soluble sodium, which is organically bounded with nitrogen- or oxygen-containing functional groups; (4) insoluble sodium, which is bounded with clay minerals.

46 The first three forms of sodium are releasable during coal combustion while the last insoluble sodium
47 remains in the residual ash due to the low activity of silicate minerals [5]. Although offline
48 measurements can detect the final amount and composition of sodium species at post-combustion stage,
49 it cannot directly capture the dynamic sodium release process and obtain the time-resolved information
50 of the sodium release rate at different coal combustion stages. To overcome these disadvantages of
51 offline techniques, online measurements using advanced laser diagnostics, e.g., Laser-Induced
52 Fragmentation Fluorescence (ELIF) [12], Tunable Diode Laser Absorption Spectroscopy (TDLAS)
53 [13], Laser-Induced Breakdown Spectroscopy (LIBS) [14] and Planar Laser-Induced Fluorescence
54 (PLIF) [15], have been recently implemented. For instance, van Eyk et al. [16] developed a PLIF
55 technique to measure the distribution of atomic Na and its time-resolved release process in the plume
56 of a burning coal particle. LIBS is a type of atomic emission spectroscopy based on the plasma
57 generated by a high power laser. The detailed principle of LIBS can be found in previous publications
58 [17, 18]. Recently, simultaneous measurement of sodium and potassium release over burning coal and
59 wood particles using this technique has been reported by Hsu et al. [19] and also in our previous work
60 [14]. However, the abovementioned studies focused on either the measurement of the distribution of
61 one sodium species, e.g., atomic Na, or the measurement of total sodium element at a single measuring
62 point. To our best knowledge, the directly time-resolved measurement of total sodium flux from a
63 burning coal particle via multi-point LIBS technique has not been reported.
64 Technologies for reducing the harmful sodium emissions can be implemented prior to, during, or
65 after the combustion process. Washing coal with water, acid solutions, or aluminum salt solutions can
66 reduce the content of sodium compounds prior to combustion [20, 21]. In coal gasification, sorbent
67 filters can be used to clean the product gases and remove sodium compounds [22, 23]. On the other

hand, pulverized-sorbents can be injected into boilers along with pulverized-coal as additives to reduce sodium release from the coal during combustion. Since this method can be directly applied in the current combustion systems without any major reconfiguration, it has attracted a lot of attentions [24-32]. Previous studies on additives for the retention of sodium release found that silica (SiO_2) and alumina (Al_2O_3) are the two important and effective compounds. Lee and Johnson [24] investigated sodium retention in pressurized fluidized bed gasification (PFBG), and their study showed that activated bauxite (81.5% Al_2O_3, 10.0% SiO_2) can retain 98% of volatilized NaCl. Punjak and Shadman [25] studied the effects of kaolin and bauxite on sodium retention, and they found that the retention by kaolin is irreversible. Takuwa and Naruse [26] further investigated the sodium retention by kaolin via a drop tube furnace. It was suggested that NaOH is the major sodium species it the coal used and can be reduced by reacting with Al_2O_3 in kaolin. Kosminski et al. [29] noted that molten sodium carbonate is the dominate sodium species between 800 ^oC and 850 ^oC in the low-rank coal and silica can react with it to reduce sodium release.

Kyi and Chadwick [27] evaluated the performance of various additives, e.g., silica (diatomite), alumina, calcium silicate (wollastonite), mine overburden, and various aluminosilicates with different alumina/silica ratios on the sodium retention of different coals. From their results and previous studies [24, 26], the reactions of sodium retention can be summarized as follows:

For NaCl:

$$2NaCl + nSiO_2 + H_2O \rightarrow Na_2O{\cdot}nSiO_2 + 2HCl \quad (1)$$

$$2NaCl + Al_2O_3{\cdot}2SiO_2 + H_2O \rightarrow Na_2O{\cdot}Al_2O_3{\cdot}2SiO_2 + 2HCl \quad (2)$$

$$2NaCl + Al_2O_3 + H_2O \rightarrow 2NaAlO_2 + 2HCl \quad (3)$$

For NaOH:

$$2NaOH + nSiO_2 \rightarrow Na_2O \cdot nSiO_2 + H_2O \quad (4)$$

$$2NaOH + Al_2O_3 \cdot 2SiO_2 \rightarrow Na_2O \cdot Al_2O_3 \cdot 2SiO_2 + H_2O \quad (5)$$

$$2NaOH + Al_2O_3 \rightarrow 2NaAlO_2 + H_2O \quad (6)$$

For $NaSO_4$:

$$Na_2SO_4 + nSiO_2 \rightarrow Na_2O \cdot nSiO_2 + SO_3 \quad (7)$$

$$Na_2SO_4 + Al_2O_3 \cdot 2SiO_2 \rightarrow Na_2O \cdot Al_2O_3 \cdot 2SiO_2 + SO_3 \quad (8)$$

$$Na_2SO_4 + Al_2O_3 \rightarrow 2NaAlO_2 + SO_3 \quad (9)$$

The abovementioned previous studies on additives for sodium retention employed offline measurements to monitor the amount of sodium released, and therefore there is no information about the temporal release characteristics of sodium for coal blended with additives. Moreover, the sodium retention performance of additives at different stages of coal combustion has rarely been revealed yet.

In our previous work [33], single point LIBS measurements were performed to obtain the gaseous sodium concentration at one fixed position during the combustion of Zhundong coal blended with different additives. In the present study, the performance of different sorbent additives on the release of sodium during the combustion of Zhundong coal will be investigated by combined online- and offline-measurements. Online multi-point LIBS technique, upgraded from the single point LIBS, will be employed for the in-situ measurement of the time-resolved sodium release flux of the coal and coal/additives mixtures. Offline techniques, which include inductively coupled plasma atomic emission spectrometer (ICP-AES), X-ray diffraction, and ash fusion temperatures (AFTs), will be applied to investigate the individual behavior of each sodium class and the influence of additives on the compositions and slagging characteristics of residual ash. The offline ICP-AES results will serve as a reference to verify the online quantitative multi-point LIBS measurements. Based on these

112 experiments, the advantage and disadvantages of different additives for sodium retention of Zhundong
113 coal have been discussed.
114 The paper is organized as follows: details on the online- and offline-measurement methods are
115 presented in Section 2. Global sodium retention characteristics of different additives revealed from the
116 offline ICP-AES measurements are illustrated in Section 3.1. The temporal sodium release
117 characteristics of different blended coal/additive pellets obtained using the online multi-point LIBS
118 technique are discussed in Section 3.2. The subsequent Section 3.3 is devoted to analyze the effects of
119 additives on the chemical compositions and AFTs of residual ash. Finally, the findings of this paper
120 are summarized in Section 4.
121
122 **2. Experimental**
123 *2.1. Coal and mineral additives*
124 A typical Chinese brown coal called Zhundong coal [5, 8, 33-36], which has appreciable sodium
125 content, is considered in the present study. The results of proximate analysis and ultimate analysis, as
126 well as the ash composition of the coal sample are listed in Table 1. Proximate analyses were performed
127 by chemical analysis methods according to the Chinese National Standard GB/T 212-2008. Ultimate
128 analyses were determined according to the Chinese National Standard GB/T 476-2008 (for C, H),
129 GB/T 19227-2008 (for N) and GB/T 214-2007 (for S). The mass fraction of oxygen (O) was
130 determined by 100%-C%-H%-N%-S%. Ash compositions were determined according to the Chinese
131 National Standard GB/T 1574-2007. Different additives were blended with Zhundong coal to explore
132 their effects on sodium retention. Specifically, typical natural mineral additives, i.e., kaolin, mica and
133 pyrophyllite, and pure silica and alumina are employed. The physical and chemical properties of these

additives are summarized in Table 2. All the additives are blended with the coal at a dosing ratio of 3% by weight, which is a typical dose for sorbents [33]. The mixing process of coal and additives is as follows. Coal and additives are first grounded and sieved to a fine powder (<75 μm). Then they are mixed according to the dosing ratio in a grinder of 32,000 rpm for 5 minutes to produce coal-additive mixture powder.

Table 1. Chemical analysis of Zhundong coal.

Proximate analysis (wt%, air dry basis)						
Moisture	Ash	Volatile	Fix Carbon			
9.85	4.23	28.72	57.2			
Ultimate analysis (wt%, dry ash free basis)						
Carbon	Hydrogen	Nitrogen	Sulfur	Oxygen		
79.29	2.89	0.88	0.43	16.5		
Ash composition (wt%)						
SiO_2	Al_2O_3	Fe_2O_3	CaO	MgO	K_2O	Na_2O
10.80	9.62	3.95	36.82	9.20	0.40	10.87

Table 2. Physical and chemical properties of the additives.

	Silica	Alumina	Kaolin	Mica	Pyrophyllite
Dimensional parameter					
Surface area (m^2/g)	0.3	173	7.8	3.1	4.5
Pore volume (cm^3/g)	0.002	0.244	0.037	0.012	0.019

Mean pore diameter (nm)	18.6	5.6	18.7	16.2	16.4
Chemical composition (wt %)					
Al_2O_3		>99	21.54	25.54	29.38
SiO_2	>99		66.64	65.49	60.20
Na_2O			0.18	0.73	0.21
CaO			0.12	0.18	0.13
MgO			0.43	2.06	0.43
Fe_2O_3			0.27	2.25	0.34
K_2O			0.19	5.24	0.06

146

147 *2.2. Ash fusion temperature and X-ray diffraction analysis*

148 The ash fusion temperatures (AFTs) are determined via an ash melting point apparatus according
149 to the GB/T 219-2008 standard. Ash samples are first grounded to powders with an diameter of less
150 than 100 μm, and then pressed into a pyrometric cone. The cone has a height of 20 mm and a equilateral
151 triangle of 7 mm at the bottom. An auto-analyzer heats up the pyrometric cone with a heating rate of
152 15–20 ºC/min under 900 ºC and 5 ºC/min above 900 ºC. The atmosphere inside the auto-analyzer
153 consists of CO and CO_2 at a mole ratio of 1:1. Four characteristic temperatures of the ash samples can
154 then be obtained, i.e., deformation temperature (DT), soft temperature (ST), hemisphere temperature
155 (HT) and fluid temperature (FT).

156 The mineral structures of the ash samples are detected using X-ray diffraction (XRD)
157 measurements, which are recorded on a Rigaku D/max 2550PC diffractometer using Cu Kα radiation.
158 The measurements are operated at 40 KV/40 mA with a scanning rate of 4 º/min in the range of 2θ =
159 20º–80º.

2.3. Identification of sodium classes

Different classes of sodium are identified according to their solubility in different solvents via a chemical fractionation method. 1 g of the coal sample was first added into 100 ml water at 333 K and stirred for 24 hours. The mixture is filtered afterwards. Inductively coupled plasmas atomic emission spectroscopy (ICP-AES) is used to analyze the filtrate to identify the content of first class water-soluble sodium like sodium sulfates and chlorides. The solid filter residue is then sequentially dissolved in 100 ml NH_4Ac (1 mol/L) and 100 ml HCl (1 mol/L), with the filtrate of each case analyzed using ICP-AES. This analysis is able to identify the second class of sodium organically bounded with carboxyl groups, and the third class organically bounded with nitrogen- or oxygen-containing functional groups. The final residue after HCl extraction is digested in strong acid and also analyzed via ICP-AES to obtain the information of the last class non-soluble sodium, such as sodium silicate.

2.4. Multi-point LIBS measurement system

The coal and additives are first grounded and sieved to a fine powder (<75 μm). Then they are blended at the desired mass ratio (97% coal and 3% additives). 50 mg of the coal/additive mixture is pressed into a 4 mm spherical pellet.

The configuration of the multi-point LIBS measurement system is shown in Fig. 1a. A spherical coal pellet is suspended on two ceramic rods (diameter of 1 mm) at a height of 10 mm above a heat flux burner. The burner produces a laminar premixed methane/air flame at an equivalence ratio of 0.8 with the flow rates of methane and air at 0.59 SL/min and 7.06 SL/min, respectively. Based on CHEMKIN simulation of the flame with GRI-3.0 mechanism, the temperature at the pellet height is estimated to be ~1892 K with the following primary gas composition: 3.9% O_2, 7.6% CO_2, 15.4% H_2O and 72.8% N_2.

An Nd:YAG laser (Spectra Physics, Model PRO-250) with a fundamental wavelength of 1064 nm is focused into the gas plume 10 mm above the burning coal pellet. The repetition rate, pulse duration and average laser energy are 10 Hz, 10 ns and 300 mJ, respectively. The LIBS signal is collected by an Ocean Optics spectrometer (Model USB 4000). The laser and spectrometer are synchronized via a digital pulse generator (Stanford Research System, DG535). The laser focusing lens and LIBS signal collection optics are installed on an electric translational platform to perform multi-point LIBS measurement (Fig. 1b). The LIBS measuring point is moving periodically in the radius distance (r) of -12 mm, -9 mm, -6 mm, -3 mm, 0 mm, 3 mm, 6 mm, 9 mm, 12mm. The moving frequency of the platform is 10 Hz, while the LIBS measuring frequency at the same point is 1 Hz.

To quantify the sodium concentration, the LIBS system has been calibrated by measuring the intensity of the sodium doublet (588.995 nm and 589.592 nm) in an NaCl seeded flame. The detailed calibration procedure can be found in our previous study [36]. The obtained linear response of LIBS signal to sodium concentration is:

$$I_{LIBS,Na} = 2430 \times C_{Na},\ R^2 = 0.96 \tag{10}$$

where $I_{LIBS,Na}$ is the LIBS signal intensity of sodium and C_{Na} is the sodium concentration at the measuring point.

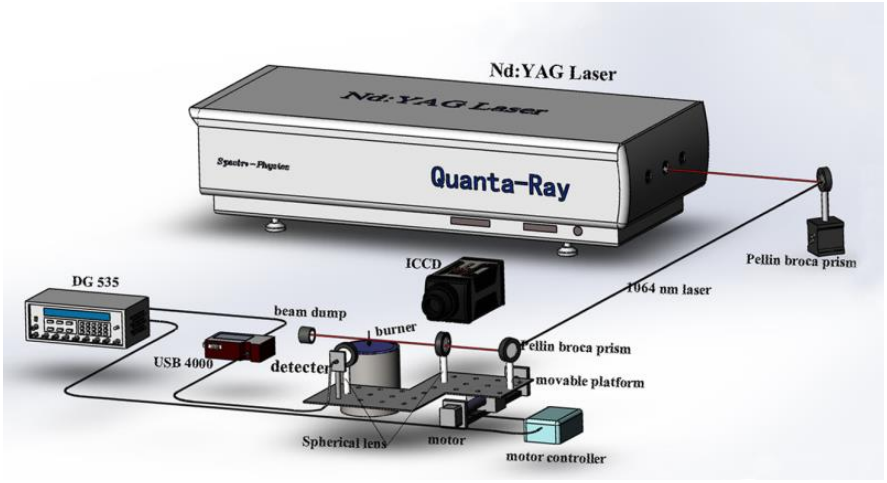

(a) Configeration of equipments

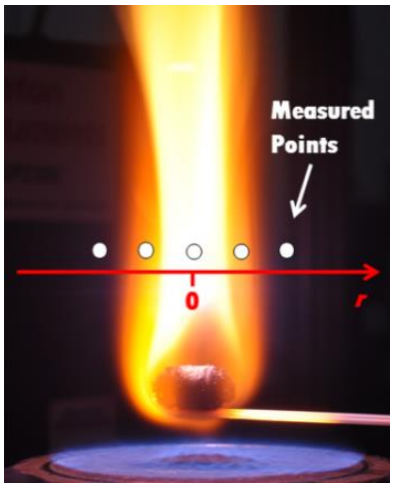

(b) LIBS measuring points

198 Fig. 1. Multi-point LIBS experimental setup.

199

200 Based on the sodium concentration of all the measuring points, the flux of sodium ($Na_{flux,t}$) passing
201 through the horizontal plane 10 mm above the burning coal pellet can be determined as:

202 $$Na_{flux,t} = \int_0^{2\pi} \int_0^{\infty} u \times C_{Na} \times r \times dr \times d\theta \quad (11)$$

203 where u is the axial velocity and θ is the radian. In the present study, the pellet is spherical and burned
204 in a uniform gas flow provided by the burner. Hence, Eq. (11) can be simplified as:

205 $$Na_{flux,t} = 2\pi \times \int_0^{\infty} u \times C_{Na} \times r \times dr \quad (12)$$

206 Since the distributions of u and C_{Na} are functions of the radial distance r, the $Na_{flux,t}$ at a given time can
207 be written as:

208 $$u = f_u(r) \quad (13)$$

209 $$C_{Na} = f_{Na,t}(r) \quad (14)$$

210 $$Na_{flux,t} = 2\pi \times \int_0^{\infty} f_t(r) \times dr \quad (15)$$

211 The sodium flux $Na_{flux,t}$ at a given combustion time can be obtained by performing an integration of a
212 function of r. In addition, the integration of the sodium flux with the combustion time can give the
213 total amount of sodium released during the burning of a coal pellet.

214 $$Na_{volatile} = \int_0^{\infty} Na_{flux,t} \times dt \quad (16)$$

215 Specifically, the measured sodium concentration at different r for a given combustion time can be fitted
216 by a two degree polynomial equation:

217 $$f_{na,t}(r) = a_2 \times r^2 + a_1 \times r + a_0 \quad (17)$$

218 Similar, the axial velocity at different r can also be fitted by a four degree polynomial equation:

219 $$f_u(r) = b_4 \times r^4 + b_3 \times r^3 + b_2 \times r^2 + b_1 \times r + b_0 \quad (18)$$

where a_2, a_1, a_0, b_4, b_3, b_2, b_1 and b_0 are the fitting coefficients.

Then the sodium release flux can be obtained by the integration of the polynomial profiles along the radius distance. More details about the fitting and integrating procedures can be found in our previous study [37].

3. Results and discussion

3.1. Global sodium retention characteristics of different additives

Pulverized Zhundong coal samples with different additives was burnt in a muffle furnace at 815 ^{o}C to produce ash according to the Chinese National Standard GB/T 1574-2007. By performing the ICP-AES measurements for the raw coal and the residual ash, the global amount of sodium released during coal combustion can be quantified.

The content of the different classes of sodium in Zhundong raw coal and the ash collected from different burnt coal samples are summarized in Table 3. The values given in the table are the mass of Na (mg) in a sample prepared from 1 g of Zhundong raw coal. Corrections have been made to account for the reduction of sodium in the sample due to the displacement of coal by sorbent additives. Each experiment is repeated three times and the average value is given along with the statistical uncertainty of the measurements. For Zhundong raw coal, the major sodium classes are water-soluble (66.8%) and insoluble (21.3%) sodium, while the content of the other two sodium classes, i.e., NH_4Ac-soluble and HCl-soluble sodium, are minor. Similar characteristics can also be observed in the ash prepared without additives. For coals with the 3% additives, the insoluble sodium (57.0%–85.9%) plays a dominant role in the 4 classes of sodium. For the sample with 3% pyrophyllite, its total sodium content is slightly higher than that in Zhundong raw coal, which could be attributed to experimental uncertainty.

Table 3. The content of different classes of sodium in Zhundong raw coal and the ashes burnt from the coal with different additives.

Sample	Na content (mg/1 g of raw coal)				
	Water-soluble	NH_4Ac-soluble	HCl-soluble	Insoluble	Total
Zhundong raw coal	4.95±0.16	0.55±0.06	0.33±0.06	1.58±0.11	7.41
Na content in the ash					
No additive	1.89±0.07	0.10±0.02	0.31±0.04	1.59±0.10	3.89
3% silica	0.79±0.03	0.70±0.08	0.55±0.07	5.05±0.25	7.09
3% alumina	0.89±0.03	0.95±0.08	1.06±0.06	3.84±0.12	6.74
3% kaolin	0.45±0.02	0.26±0.07	0.92±0.10	5.68±0.28	7.31
3% mica	0.81±0.03	0.73±0.07	0.94±0.09	4.81±0.29	7.29
3% pyrophyllite	0.29±0.01	0.26±0.04	0.51±0.07	6.39±0.26	7.45

Comparing the sodium content in the ash and the raw coal, the variation of the content of different classes of sodium before and after combustion in Zhundong coal and coal/additive blends can be obtained, as shown in Fig. 2. The average result is shown along with error bars which indicate the statistical uncertainty of the measurements. The negative value means the consume of a sodium class, which should be either released into the gas phase or transformed into other sodium classes, while the positive value means the produce of a sodium class, which should be generated from other sodium classes. For the coal with no additive, it can be found that 47.5% (Table 3) of the total sodium is released during the combustion, of which is mainly the water-soluble sodium. The contribution of NH_4Ac-soluble, HCl-soluble and insoluble sodium to the total sodium release is minor. When the coal is burnt with additives, its sodium release characteristics are clearly affected. The amount of total

sodium released during combustion has been significantly reduced after the coal is mixed with additives. Specifically, the released percentage of total sodium is 4.3%, 9.1%, 1.4%, 1.6% and 0.0% for the additive of silica, alumina, kaolin, mica and pyrophyllite, respectively. From the variation of the content of the 4 different classes of sodium, it can be deduced that the mineral additives reduce the global sodium release via reacting with the water-soluble sodium to form insoluble sodium, which is consistent to the sodium retention mechanism proposed by Kyi and Chadwick [27].

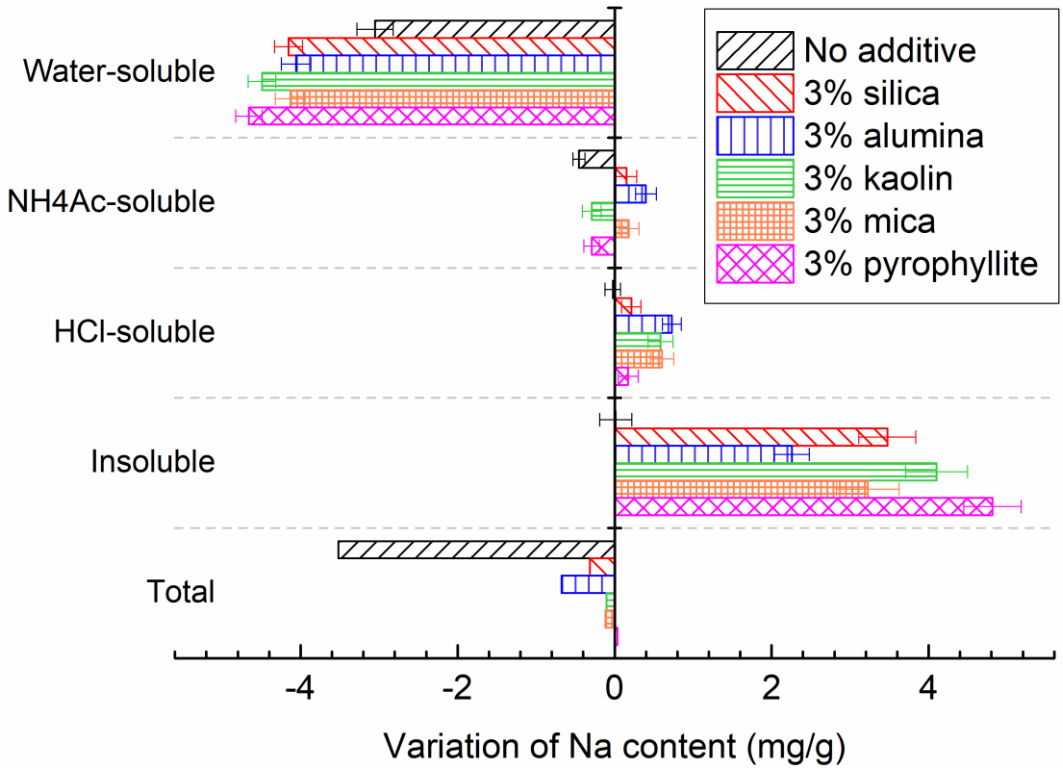

Fig. 2. Variation of the content of the different classes of sodium before and after combustion in Zhundong coal and the coal/additive blends.

3.2. In-situ measurement of temporal sodium release during combustion

LIBS technique introduced in Section 2.4 has been employed for the in-situ measurement of sodium concentration.

The obtained temporal release profiles of sodium during the combustion of Zhundong coal and coal/additive blends are shown in Fig. 3. Each measurement is repeated three times and the average result is shown along with error bars which indicate the statistical uncertainty of the measurements. The three characteristic stages of coal combustion can be clearly observed for the coal and coal/alumina samples: first, a narrow peak during the devolatilization stage; then, a left skewed large peak characterize the char burnout stage; finally, a slow decrease to baseline in the ash cooking stage. For other coal/additive blends, the sodium flux profiles exhibit slightly different characteristics. The second peak for the char burnout stage becomes less obvious, as shown in the zoomed in first 800 s of combustion time (Fig. 3). The time at termination of the three combustion stages for the 6 samples is determined and summarized in Table 4. The end point of the ash stage is the time when the average sodium signal is consistently below the baseline. It can be found that all the sorbent additives result in a longer coal burnout time. This is anticipated since the displacement of coal by sorbent additives reduce the combustible compositions in the pellet and therefore its burning rate slows down. On the other hand, the duration of sodium release in the ash stage is found to be largely decreased by the sorbent additives.

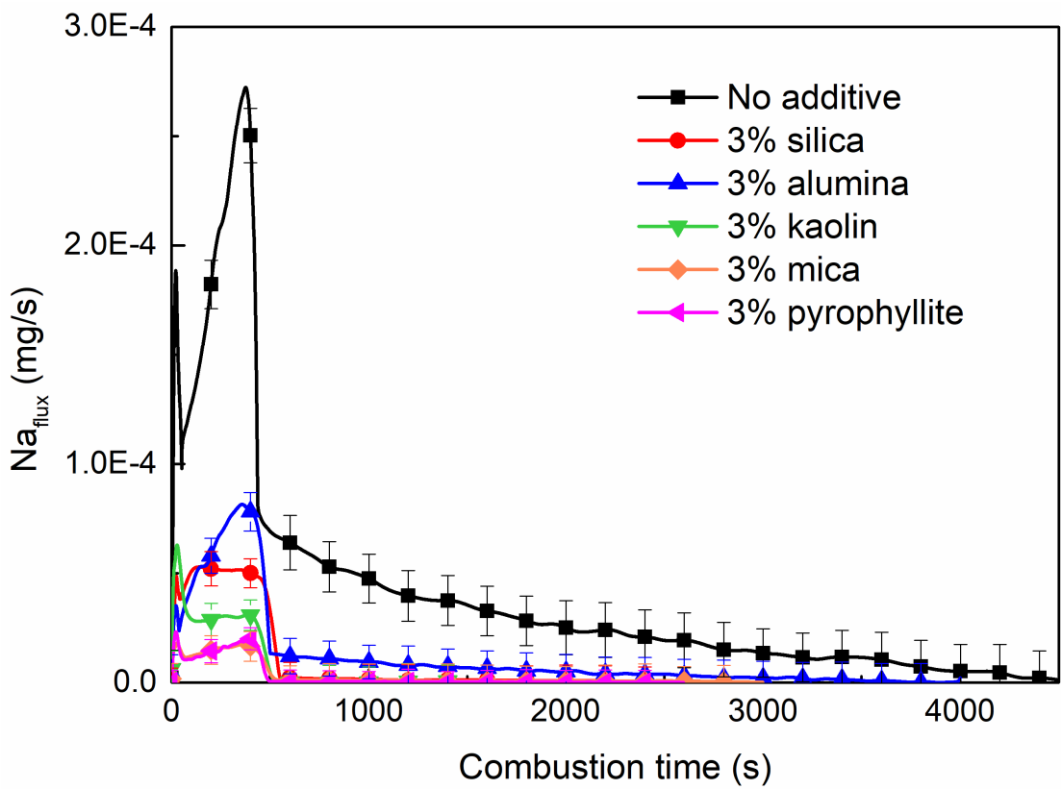
3.0E-4
2.0E-4
1.0E-4
0.0
Na_{flux} (mg/s)
0
1000
2000
3000
4000
Combustion time (s)
No additive
3% silica
3% alumina
3% kaolin
3% mica
3% pyrophyllite

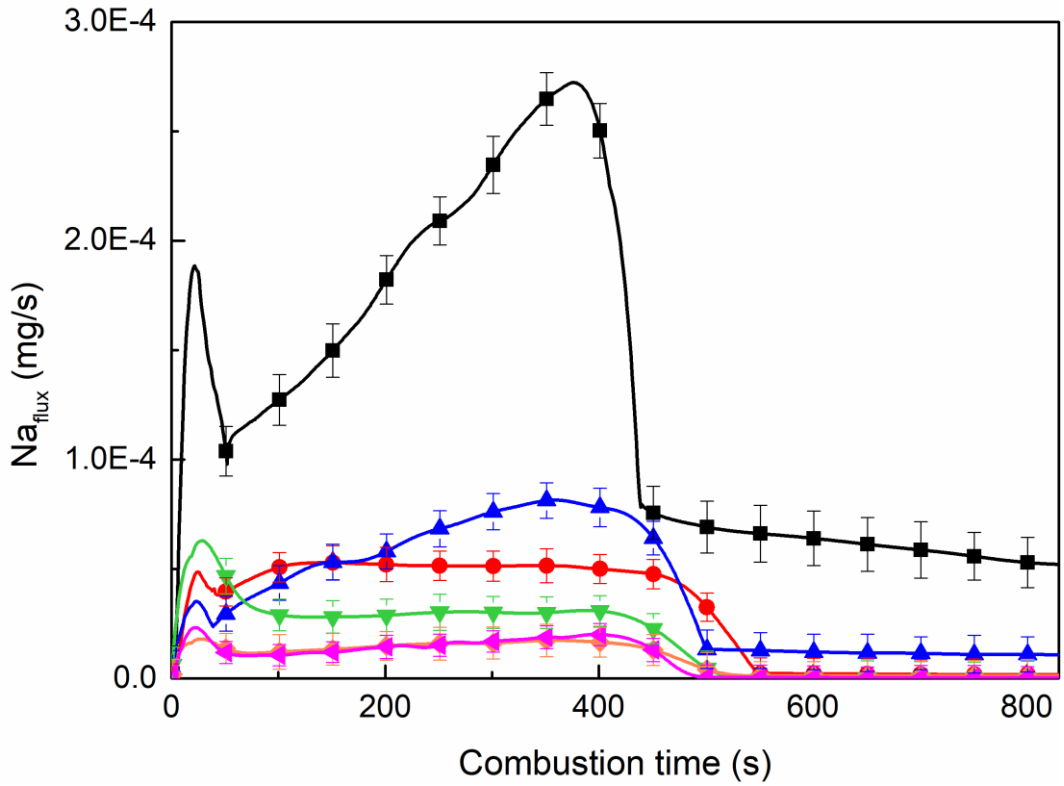

Fig. 3. Temporal sodium release profile for Zhundong coal and coal/additive blends measured by multi-point LIBS. The first 800 s of combustion time has been zoomed in and shown on the bottom side.

Table 4. Time at termination of three combustion stages for Zhundong coal and coal/additive blends.

Sample	Time at termination (s)		
	Devolatilization	Char burnout	Ash
No additive	52	439	4497
3% silica	44	551	2596
3% alumina	39	501	3877
3% kaolin	80	536	1492
3% mica	61	530	2999
3% pyrophyllite	59	500	2590

By integrating the sodium flux with the combustion time, we can obtain the amount of sodium

304 released at the three different stages of the pellet burning, as listed in Table 5. Note that the values in
305 the table have been converted for 1 g of raw coal, in order to facilitate the comparison with the ICP-
306 AES results in Section 3.1. Corrections have been made to account for the reduction of sodium in the
307 sample due to the displacement of coal by sorbent additives. For the total amount of sodium released,
308 the multi-point LIBS measurements agree well with the ICP-AES results within an error of 0.274 mg
309 per 1 g of raw coal. The small deviation could be due to the difference of combustion configurations
310 of the coal/additive blends. In multi-point LIBS experiments, the coal/additives were pressed into
311 pellets and burnt in a premixed methane/air flame, while in ICP-AES experiments the coal/additives
312 were burnt in a muffle furnace. By comparing the sodium released at the three stages for Zhundong
313 coal, it can be found that the char burnout and ash stages contribute to 41.4% and 54.9% of the total
314 sodium released, respectively, while the devolatilization stage only release a marginally amount (3.7%)
315 because of its short duration. With the additives, the sodium release during the combustion of
316 Zhundong coal is significantly reduced. Figure 4 illustrates the sodium retention efficiency of different
317 additives calculated using the results of pure coal (i.e., sample of "No additive" in Table 5) as a
318 reference. It can be found that all the five additives show significant sodium retention effects with an
319 overall retention efficiency larger than 70%. Silica is found to have a stronger sodium retention effect
320 than alumina. For the natural mineral additives, all the three minerals, i.e., kaolin, mica and
321 pyrophyllite, show a higher sodium retention efficiency than the two pure additives. Because the main
322 compounds of the three natural minerals are silica and alumina, there could be some synergistic effects
323 during the sodium retention of silica and alumina. Moreover, all the additives can effectively prohibit
324 the sodium release during the whole three stages of coal combustion, and the highest sodium retention
325 efficiency is achieved in the ash cooking stage.

Table 5. Sodium released at three stages of coal combustion for Zhundong coal and coal/additive blends.

Sample	Na released (mg/1 g of raw coal)			
	Devolatilization	Char burnout	Ash	Total
No additive	0.14	1.54	2.04	3.72
3% silica	0.03	0.48	0.05	0.56
3% alumina	0.02	0.58	0.35	0.95
3% kaolin	0.08	0.24	0.01	0.33
3% mica	0.02	0.13	0.04	0.19
3% pyrophyllite	0.02	0.13	0.02	0.17

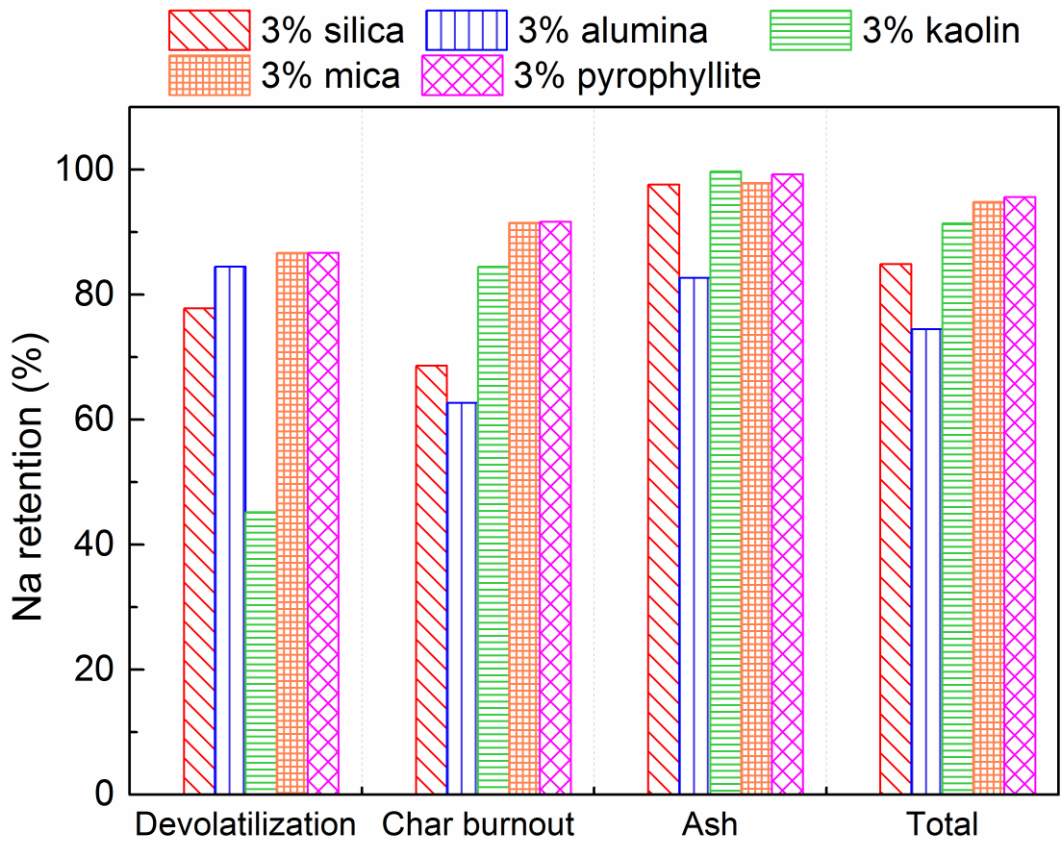

Fig. 4. Sodium retention efficiency of different additives at three stages of coal combustion.

333

334 *3.3. Effects of additives on the characteristics of residual ash*

335 The ash compositions of different samples obtained via wet chemical analysis methods according
336 to the Chinese National Standard GB/T 1574-2007 are summarized in Table 6. The variation of SiO_2
337 and Al_2O_3 content in different samples are closely related to the compositions of the additives (see
338 Table 2). The Na_2O content in different samples also indicates the sodium retention ability of the
339 different additives, which is in accord with the abovementioned ICP-AES and multi-point LIBS
340 measurements. The last column correspond to the mass of ash for the 6 different samples. It can be
341 found that the mass of ash is larger for Zhundong coal/additive blends than the sample of pure coal.
342 One reason is that the 3% additives turn into ash after burning. Meanwhile it could also be attributed
343 to the retention effects of the sorbent additives, including the sodium retention effects.

344

345 Table 6. Compositions of the residual ashes prepared from Zhundong coal and coal/additive blends.

Sample	Ash compositions (mg/1 g of raw coal)							
	SiO_2	Al_2O_3	Fe_2O_3	CaO	MgO	K_2O	Na_2O	Ash
No additive	4.59	4.09	1.68	15.65	3.91	0.17	4.62	42.50
3% silica	38.99	1.99	4.19	12.76	7.77	0.12	7.41	80.90
3% alumina	5.03	27.18	6.10	14.90	5.69	0.08	6.60	78.50
3% kaolin	28.64	10.13	6.53	15.64	7.12	0.22	8.01	86.10
3% mica	28.78	9.39	6.35	15.52	7.01	0.50	8.36	84.50
3% pyrophyllite	23.26	10.38	8.76	14.03	5.56	0.39	8.42	79.70

346

347 Figure 5 shows the chemical compositions of the residual ash of the six samples. For the original
348 Zhundong ash with no additive, the minerals include $CaSO_4$, CaO, Fe_2O_3 and $NaAlSi_3O_8$, which is

expected since Ca, Fe, Na, Al and Si are the major elements. The sample with 3% alumina shows very similar diffraction patterns to the original Zhundong ash, indicating that the alumina additive does not significantly affect the chemical structures of Zhundong ash. On the other hand, the samples with 3% silica, kaolin, mica and pyrophyllite present different diffraction patterns. Newly formed crystals, i.e., $3MgO{\cdot}4SiO_2{\cdot}H_2O$-2M, $Mg_2Al_4Si_5O_{18}$, $Na_3KAl_4Si_4O_{16}$, $K_2O{\cdot}Al_2O_3{\cdot}6SiO_2$ and $3MgO{\cdot}4SiO_2{\cdot}H_2O$-1A, can be observed. For sodium related species, $NaAlSi_3O_8$ is found in all the six samples while $Na_3KAl_4Si_4O_{16}$ only exists in the samples with kaolin, mica and pyrophyllite additives.

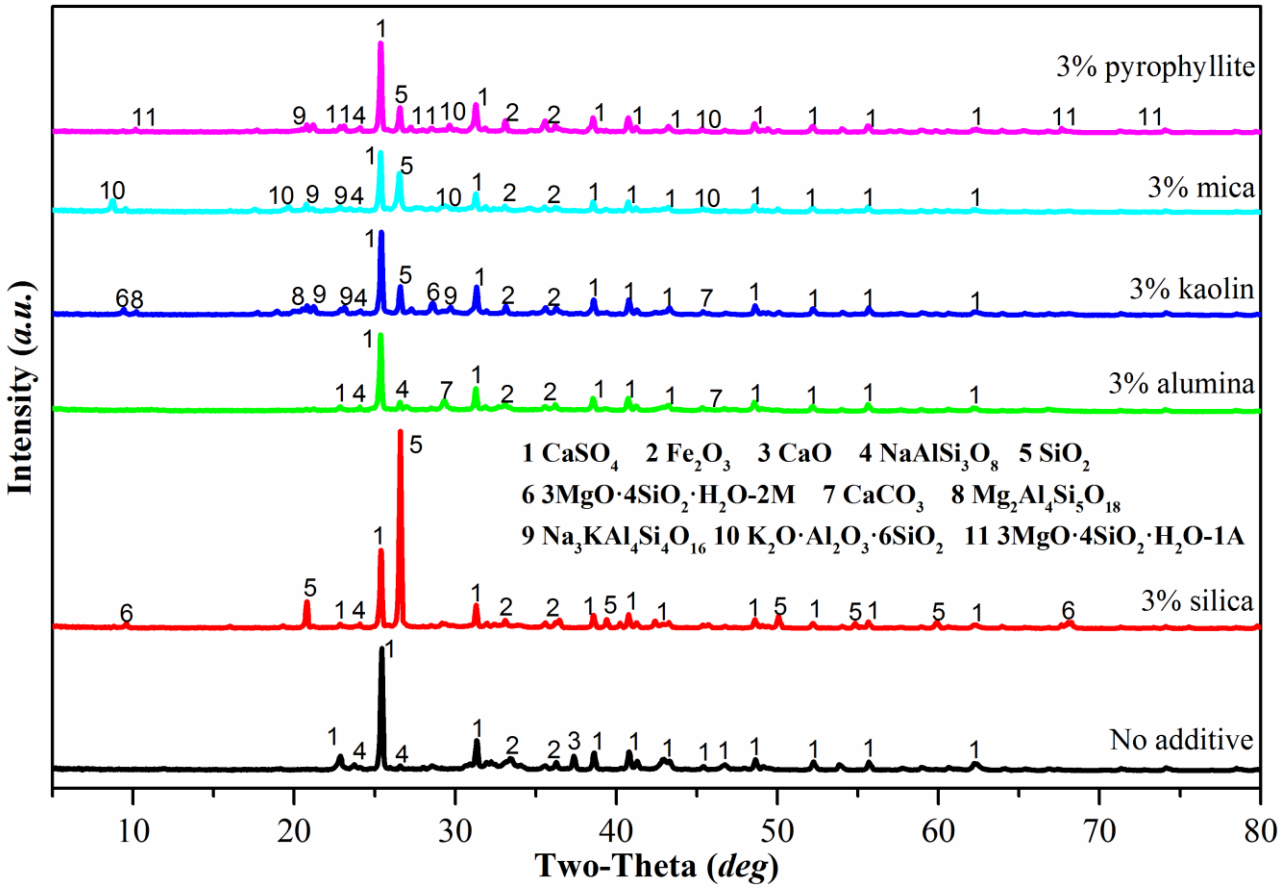

Fig. 5. XRD analysis of the ash samples prepared from Zhundong coal and coal/additive blends.

Ash fusion temperatures (AFTs) are important characteristics of the residual ash impacting the fouling and corrosion behaviors in boilers. Liquid ash is sticky and has a higher possibility to be

deposited on the heat transfer surfaces. Therefore coal with higher AFTs is helpful to relieve the fouling and corrosion issues in coal-fired boilers. To investigate the impact of various additives on the ash fusion temperatures, the deformation (DT), soft (ST), hemisphere (HT) and fluid (FT) temperatures of the six ash samples were determined and shown in Table 7. Most of the additives lead to lower AFTs, except that alumina can significantly increase the AFTs of Zhundong coal. From the XRD results, the addition of alumina has negligible effects on the chemical compositions of Zhundong ash. And alumina, itself, has a very high fusion temperature (2054 ºC), which explains this finding. For the other four additives, the chemical compositions of the residual ash are affected which implies that the new chemical structures have lower fusion temperatures.

Table 7. Ash fusion temperatures of the ash samples prepared from Zhundong coal and coal/additive blends.

Sample	Ash fusion temperatures (ºC)			
	DT	ST	HT	FT
No additive	1320	1338	1342	1347
3% silica	1305	1319	1322	1327
3% alumina	>1500	>1500	>1500	>1500
3% kaolin	1238	1271	1276	1285
3% mica	1146	1200	1204	1210
3% pyrophyllite	1127	1156	1162	1173

Besides the experimental methods, the ash fusion characteristics can also be theoretically obtained from a SiO_2-CaO-MgO-Al_2O_3 ternary phase diagram, which is calculated by using the phase diagram module in the FactSage software [38]. The mass fraction of MgO is set to a constant of 10%

during the calculation, and the obtained ternary phase diagram of SiO_2-CaO-MgO-Al_2O_3 is shown in Fig. 6. The locations of the six different ash samples are illustrated according to their own chemical compositions. It can be found that the primary crystal region is monoxide for the original Zhundong ash. With the addition of 3% silica and alumina, the primary crystal regions become diopside ($CaMgSi_2O_6$) and spinel ($MgAl_2O_4$), respectively. For the samples with 3% kaolin, mica and pyrophyllite, their primary crystal regions are all located in the zone of anorthite ($CaAl_2Si_2O_8$).

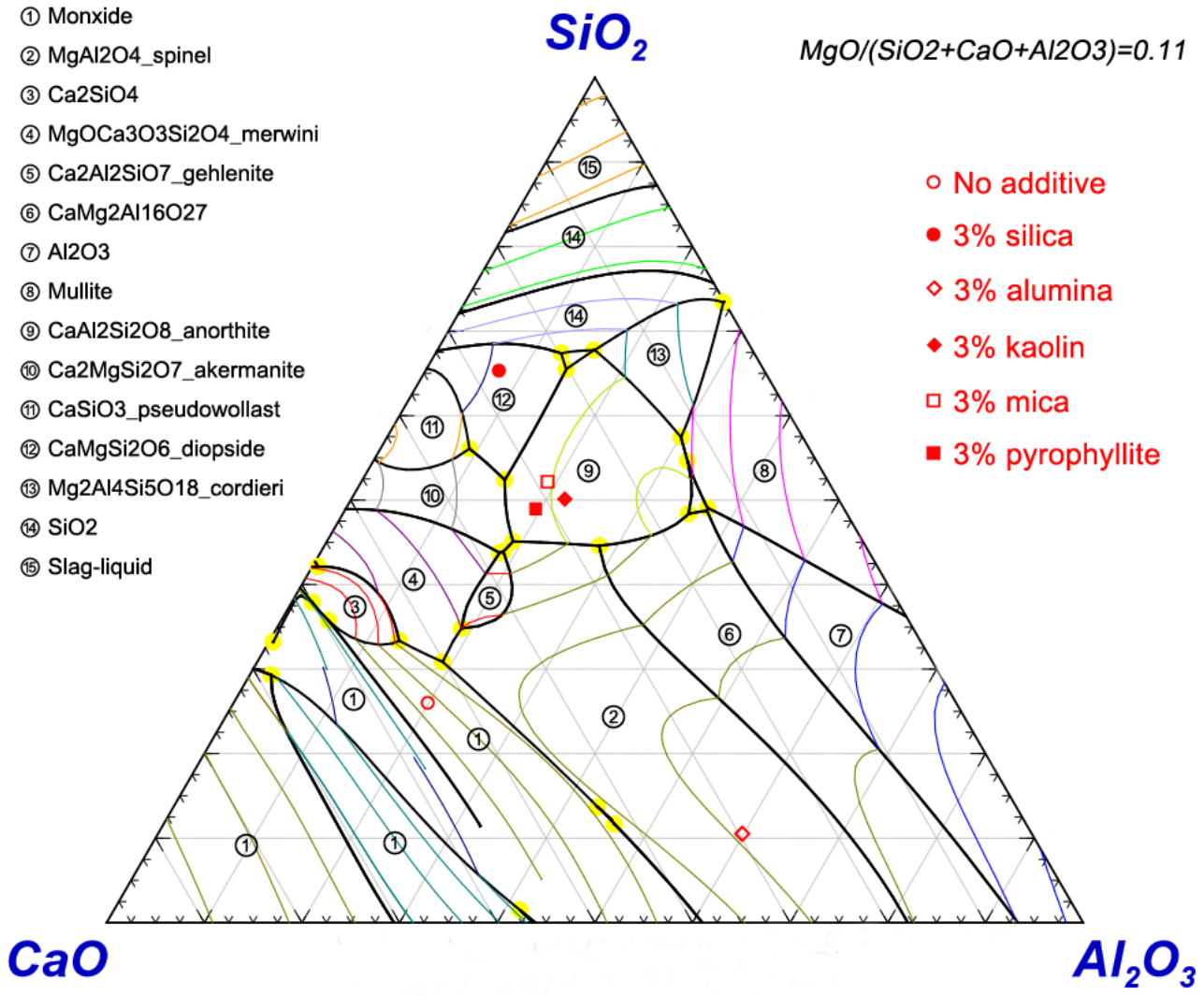

Fig. 6. SiO_2-CaO-MgO-Al_2O_3 ternary phase diagram predicted by FactSage simulations.

Figure 7 shows the liquidus temperatures of the six different ash samples predicted in the ternary phase diagram. It can be found that the sample with alumina has a much higher liquidus temperature while the other four additives lead to a lower liquidus temperature. The trend of the variation of the liquidus temperatures with different additives is consistent with the measurements of AFTs. Although, since some elements (such as Fe, K) have not been considered in the FactSage simulations, the absolute values of the predicted liquidus temperatures do not agree well with the measured AFTs. The decline of the liquidus temperatures in the samples with silica, kaolin, mica and pyrophyllite suggests the eutectic melting phenomena caused by the interactions between some crystals.

Considering both the effects of sodium retention and AFTs, alumina is more beneficial than silica to be used as additives to relieve the fouling and corrosion issues in boilers burning Zhundong coal, as it can reduce the sodium release (74.5%) and also increase the AFTs of the coal. Among the three typical natural mineral additives, kaolin is a more suitable additive since it has a good sodium retention efficiency (91.4%) and the minimal impact on decreasing the AFTs.

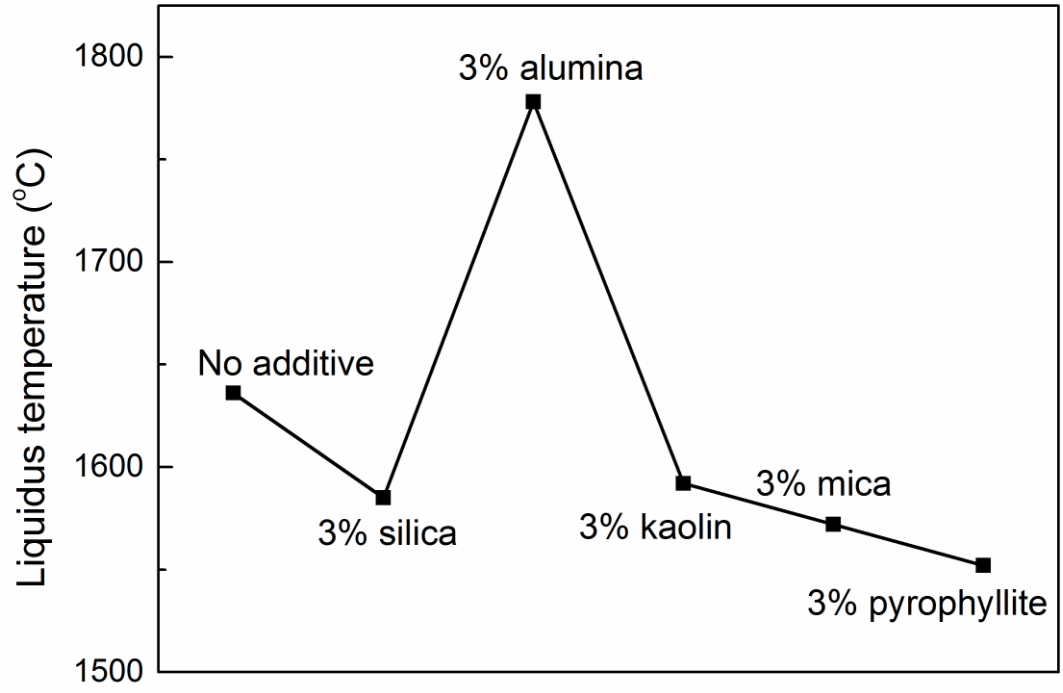

Fig. 7. Liquidus temperatures of various ash samples predicted by FactSage simulations.

4. Conclusions

The sodium retention performance of five different sorbent additives, including two pure additives, i.e., silica and alumina, and three typical natural mineral additives, i.e., kaolin, mica and pyrophyllite, for the combustion of Zhundong coal has been studied by combined online- and offline-measurements. Generally, all the five sorbent additives show a significant sodium retention effect with an overall retention efficiency larger than 70%. It is found that silica has a stronger sodium retention effect than alumina. For the natural mineral additives, all of them show higher sodium retention efficiencies than the two pure additives. Moreover, all the additives can effectively reduce sodium release during the whole three stages of coal combustion, and the highest sodium retention efficiency is achieved in the ash cooking stage. The additives are found to reduce the global sodium release via reacting with the water-soluble sodium to form insoluble sodium.

However, most of the additives lead to lower AFTs, which indicates the ash has a higher possibility to be deposited on heat transfer surfaces, except for alumina. Therefore, alumina should be a better additive than silica in relieving the fouling issues of Zhundong coal, as it can reduce the sodium release (74.5%) and increase the AFTs. Among the three natural mineral additives, kaolin has a good sodium retention efficiency (91.4%) and the minimal impact on decreasing the AFTs.

Acknowledgements

This work was supported by the National Natural Science Foundation of China (51422605, 51621005) and the Fundamental Research Funds for the Central Universities (2016QNA4013).

425

426 **References**

427 [1] Khatami R, Levendis YA. An overview of coal rank influence on ignition and combustion
428 phenomena at the particle level. Combust. Flame 2016;164:22-34.
429 [2] Wan KD, Xia J, Wang ZH, Pourkashanian M, Cen KF. Large-eddy Simulation of Pilot-assisted
430 Pulverized-coal Combustion in a Weakly Turbulent Jet. Flow Turbul. Combust. 2017;99(2):531-
431 50.
432 [3] Wan KD, Xia J, Wang ZH, Wrobel LC, Cen KF. Online-CPD-coupled large-eddy simulation of
433 pulverized-coal pyrolysis in a hot turbulent nitrogen jet. Combust. Sci. Technol. 2017;189(1):103-
434 31.
435 [4] Jiang S, Shen L, Niu X, Ge H, Gu H. Chemical Looping Co-combustion of Sewage Sludge and
436 Zhundong Coal with Natural Hematite as the Oxygen Carrier. Energy Fuels 2016;30(3):1720-9.
437 [5] He Y, Qiu KZ, Whiddon R, Wang ZH, Zhu YQ, Liu YZ, et al. Release characteristic of different
438 classes of sodium during combustion of Zhun-Dong coal investigated by laser-induced
439 breakdown spectroscopy. Sci. Bull. 2015;60(22):1927-34.
440 [6] Wu X, Zhang X, Yan K, Chen N, Zhang J, Xu X, et al. Ash deposition and slagging behavior of
441 Chinese Xinjiang high-alkali coal in 3 MWth pilot-scale combustion test. Fuel 2016;181:1191-
442 202.
443 [7] Song G, Qi X, Song W, Lu Q. Slagging Characteristics of Zhundong Coal during Circulating
444 Fluidized Bed Gasification. Energy Fuels 2016;30(5):3967-74.
445 [8] Wang ZH, Liu YZ, Whiddon R, Wan KD, He Y, Xia J, et al. Measurement of atomic sodium release
446 during pyrolysis and combustion of sodium-enriched Zhundong coal pellet. Combust. Flame
447 2017;176:429-38.
448 [9] Quann RJ, Neville M, Janghorbani M, Mims CA, Sarofim AF. Mineral matter and trace-element
449 vaporization in a laboratory-pulverized coal combustion system. Environ. Sci. Technol.
450 1982;16(11):776-81.
451 [10] Benson SA, Holm PL. Comparison of inorganic constituents in three low-rank coals. Ind. Eng.
452 Chem., Prod. Res. Dev.;(United States) 1985;24(1).
453 [11] Zhang J, Han C-L, Yan Z, Liu K, Xu Y, Sheng C-D, et al. The Varying Characterization of Alkali

Metals (Na, K) from Coal during the Initial Stage of Coal Combustion. Energy Fuels 2001;15(4):786-93.

[12] Greger F, Hartinger KT, Monkhouse PB, Wolfrum J, Baumann H, Bonn B. In situ alkali concentration measurements in a pressuried, fluidized-bed coal combustor by excimer laser induced fragmentation fluorescence. Symp. (Int.) Combust. 1996;26(2):3301-7.

[13] Schlosser E, Fernholz T, Teichert H, Ebert V. In situ detection of potassium atoms in high-temperature coal-combustion systems using near-infrared-diode lasers. Spectroc. Acta Pt. A-Molec. 2002;58(11):2347-59.

[14] He Y, Zhu J, Li B, Wang Z, Li Z, Aldén M, et al. In-situ Measurement of Sodium and Potassium Release during Oxy-Fuel Combustion of Lignite using Laser-Induced Breakdown Spectroscopy: Effects of O2 and CO2 Concentration. Energy & Fuels 2013;27(2):1123-30.

[15] van Eyk PJ, Ashman PJ, Alwahabi ZT, Nathan GJ. Quantitative measurement of atomic sodium in the plume of a single burning coal particle. Combust. Flame 2008;155(3):529-37.

[16] van Eyk PJ, Ashman PJ, Alwahabi ZT, Nathan GJ. Simultaneous measurements of the release of atomic sodium, particle diameter and particle temperature for a single burning coal particle. Proc. Combust. Inst. 2009;32(2):2099-106.

[17] Rusak DA, Castle BC, Smith BW, Winefordner JD. Fundamentals and Applications of Laser-Induced Breakdown Spectroscopy. Critical Reviews in Analytical Chemistry 1997;27(4):257-90.

[18] Song K, Lee Y-I, Sneddon J. Applications of Laser-Induced Breakdown Spectrometry. Applied Spectroscopy Reviews 1997;32(3):183-235.

[19] Hsu L-J, Alwahabi ZT, Nathan GJ, Li Y, Li ZS, Aldén M. Sodium and Potassium Released from Burning Particles of Brown Coal and Pine Wood in a Laminar Premixed Methane Flame Using Quantitative Laser-Induced Breakdown Spectroscopy. Appl. Spectrosc. 2011;65(6):684-91.

[20] Vuthaluru HB, Linjewile TM, Zhang D-k, Manzoori AR. Investigations into the control of agglomeration and defluidisation during fluidised-bed combustion of low-rank coals. Fuel 1999;78(4):419-25.

[21] Vuthaluru HB, Domazetis G, Wall TF, Vleeskens JM. Reducing fly ash deposition by pretreatment of brown coal: Effect of aluminium on ash character. Fuel Process. Technol. 1996;46(2):117-32.

[22] Escobar I, Müller M. Alkali Removal at about 1400 °C for the Pressurized Pulverized Coal Combustion Combined Cycle. 2. Sorbents and Sorption Mechanisms. Energy Fuels

484 2007;21(2):735-43.
485 [23] Wang L, Hustad JE, Skreiberg Ø, Skjevrak G, Grønli M. A Critical Review on Additives to Reduce
486 Ash Related Operation Problems in Biomass Combustion Applications. Energy Procedia
487 2012;20:20-9.
488 [24] Lee SHD, Johnson I. Removal of Gaseous Alkali Metal Compounds from Hot Flue Gas by
489 Particulate Sorbents. Journal of Engineering for Power 1980;102(2):397-402.
490 [25] Punjak WA, Shadman F. Aluminosilicate sorbents for control of alkali vapors during coal
491 combustion and gasification. Energy Fuels 1988;2(5):702-8.
492 [26] Takuwa T, Naruse I. Emission control of sodium compounds and their formation mechanisms
493 during coal combustion. Proc. Combust. Inst. 2007;31 II:2863-70.
494 [27] Kyi S, Chadwick BL. Screening of potential mineral additives for use as fouling preventatives in
495 Victorian brown coal combustion. Fuel 1999;78(7):845-55.
496 [28] Vuthaluru HB, Vleeskens JM, Wall TF. Reducing fouling from brown coals by sodium-binding
497 additives. Fuel Process. Technol. 1998;55(2):161-73.
498 [29] Kosminski A, Ross DP, Agnew JB. Reactions between sodium and kaolin during gasification of
499 a low-rank coal. Fuel Process. Technol. 2006;87(12):1051-62.
500 [30] Tran KQ, Iisa K, Steenari BM, Lindqvist O. A kinetic study of gaseous alkali capture by kaolin in
501 the fixed bed reactor equipped with an alkali detector. Fuel 2005;84(2-3):169-75.
502 [31] Uberoi M, Punjak WA, Shadman F. The kinetics and mechanism of alkali removal from flue gases
503 by solid sorbents. Prog. Energy Combust. Sci. 1990;16(4):205-11.
504 [32] Zheng Y, Jensen PA, Jensen AD. A kinetic study of gaseous potassium capture by coal minerals
505 in a high temperature fixed-bed reactor. Fuel 2008;87(15-16):3304-12.
506 [33] He Y, Whiddon R, Wang ZH, Liu YZ, Zhu YQ, Liu JZ, et al. Inhibition of Sodium Release from
507 Zhundong Coal via the Addition of Mineral Additives: Online Combustion Measurement with
508 Laser-Induced Breakdown Spectroscopy (LIBS). Energy Fuels 2017;31(2):1082-90.
509 [34] Wan KD, Wang ZH, He Y, Xia J, Zhou ZJ, Zhou JH, et al. Experimental and modeling study of
510 pyrolysis of coal, biomass and blended coal–biomass particles. Fuel 2015;139:356-64.
511 [35] Wang ZH, Wan KD, Xia J, He Y, Liu YZ, Liu JZ. Pyrolysis Characteristics of Coal, Biomass, and
512 Coal–Biomass Blends under High Heating Rate Conditions: Effects of Particle Diameter, Fuel
513 Type, and Mixing Conditions. Energy Fuels 2015;29(8):5036-46.

514 [36] He Y, Zhu JJ, Li B, Wang ZH, Li ZS, Aldén M, et al. In-situ measurement of sodium and potassium
515 release during oxy-fuel combustion of lignite using laser-induced breakdown spectroscopy:
516 effects of O2 and CO2 concentration. Energy Fuels 2013;27(2):1123-30.
517 [37] Liu YZ, He Y, Wang ZH, Wan KD, Xia J, Liu JZ, et al. Measurement and kinetics of sodium
518 release from a burning Zhundong coal particle. Combust. Flame 2017;(under review).
519 [38] Bale CW, Chartrand P, Degterov SA, Eriksson G, Hack K, Ben Mahfoud R, et al. FactSage
520 thermochemical software and databases. Calphad 2002;26(2):189-228.

Figure captions

Fig. 1. Multi-point LIBS experimental setup.

Fig. 2. Variation of the content of the different classes of sodium before and after combustion in Zhundong coal and the coal/additive blends.

Fig. 3. Temporal sodium release profile for Zhundong coal and coal/additive blends measured by multi-point LIBS. The first 800 s of combustion time has been zoomed in and shown on the bottom side.

Fig. 4. Sodium retention efficiency of different additives at three stages of coal combustion.

Fig. 5. XRD analysis of the ash samples prepared from Zhundong coal and coal/additive blends.

Fig. 6. SiO_2-CaO-MgO-Al_2O_3 ternary phase diagram predicted by FactSage simulations.

Fig. 7. Liquidus temperatures of various ash samples predicted by FactSage simulations.

Color figures can be used for the online PDF version and the gray style for hardcopy reproduction.

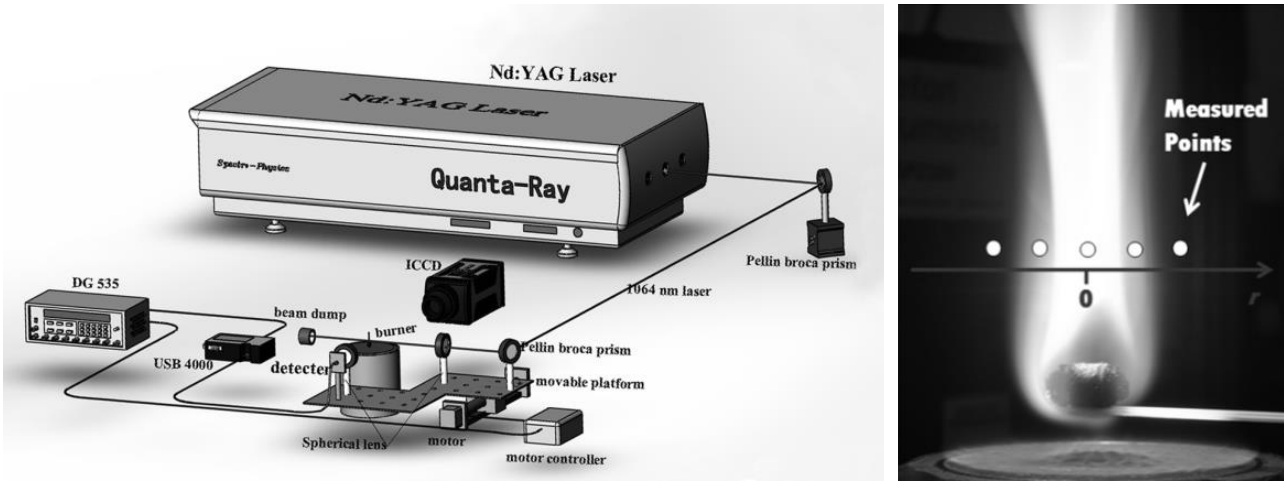

(a) Configeration of equipments (b) LIBS measuring points

Fig. 1. Multi-point LIBS experimental setup.

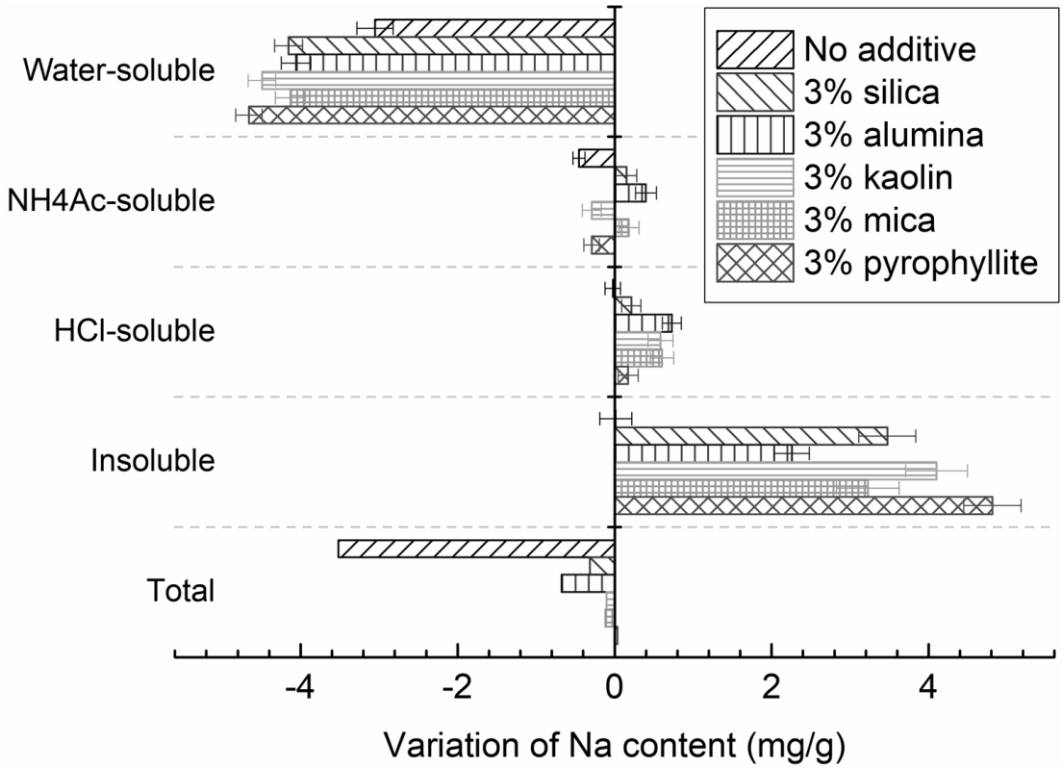

Fig. 2. Variation of the content of the different classes of sodium before and after combustion in Zhundong coal and the coal/additive blends.

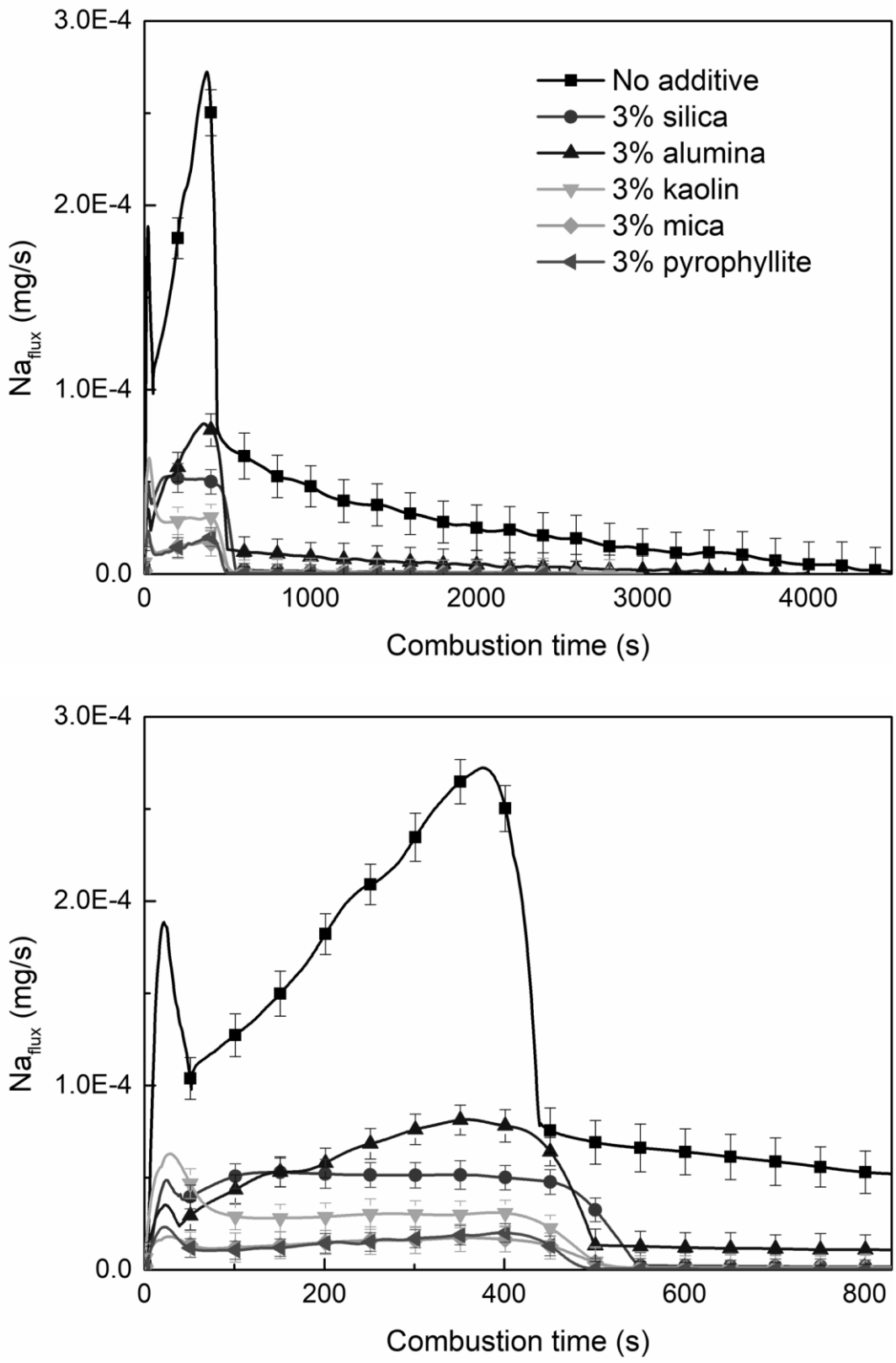

Fig. 3. Temporal sodium release profile for Zhundong coal and coal/additive blends measured by multi-point LIBS. The first 800 s of combustion time has been zoomed in and shown on the bottom side.

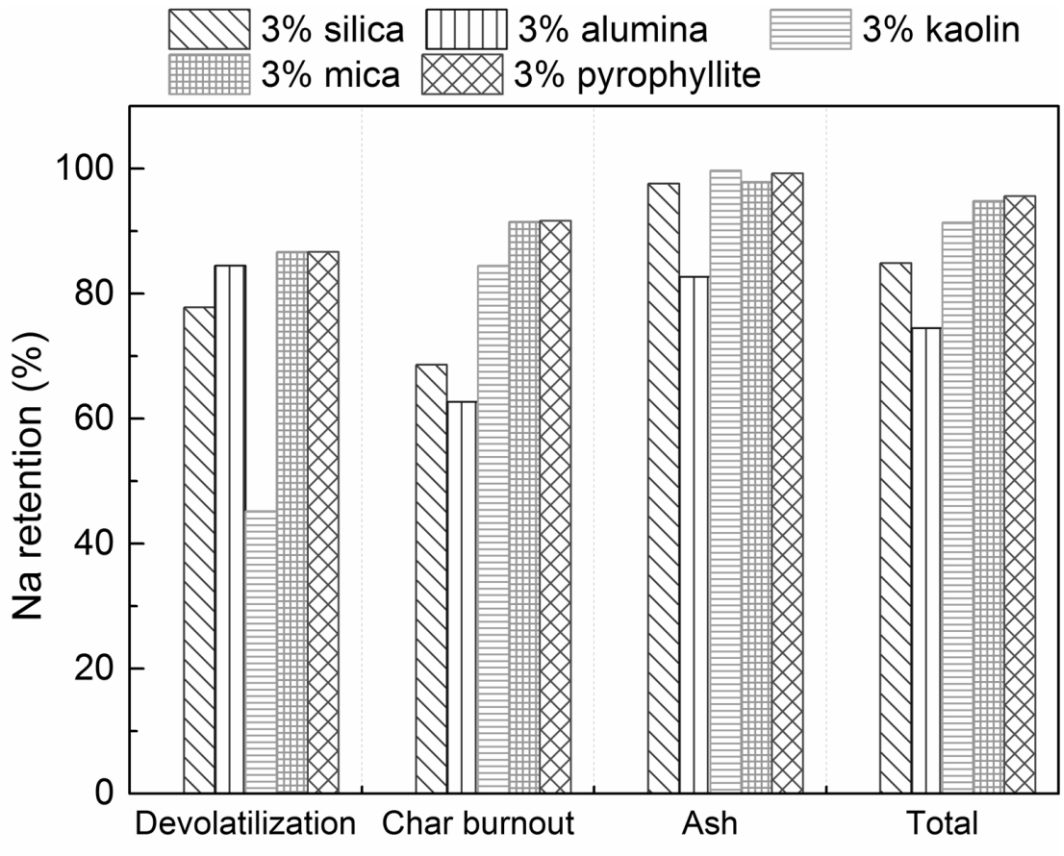

Fig. 4. Sodium retention efficiency of different additives at three stages of coal combustion.

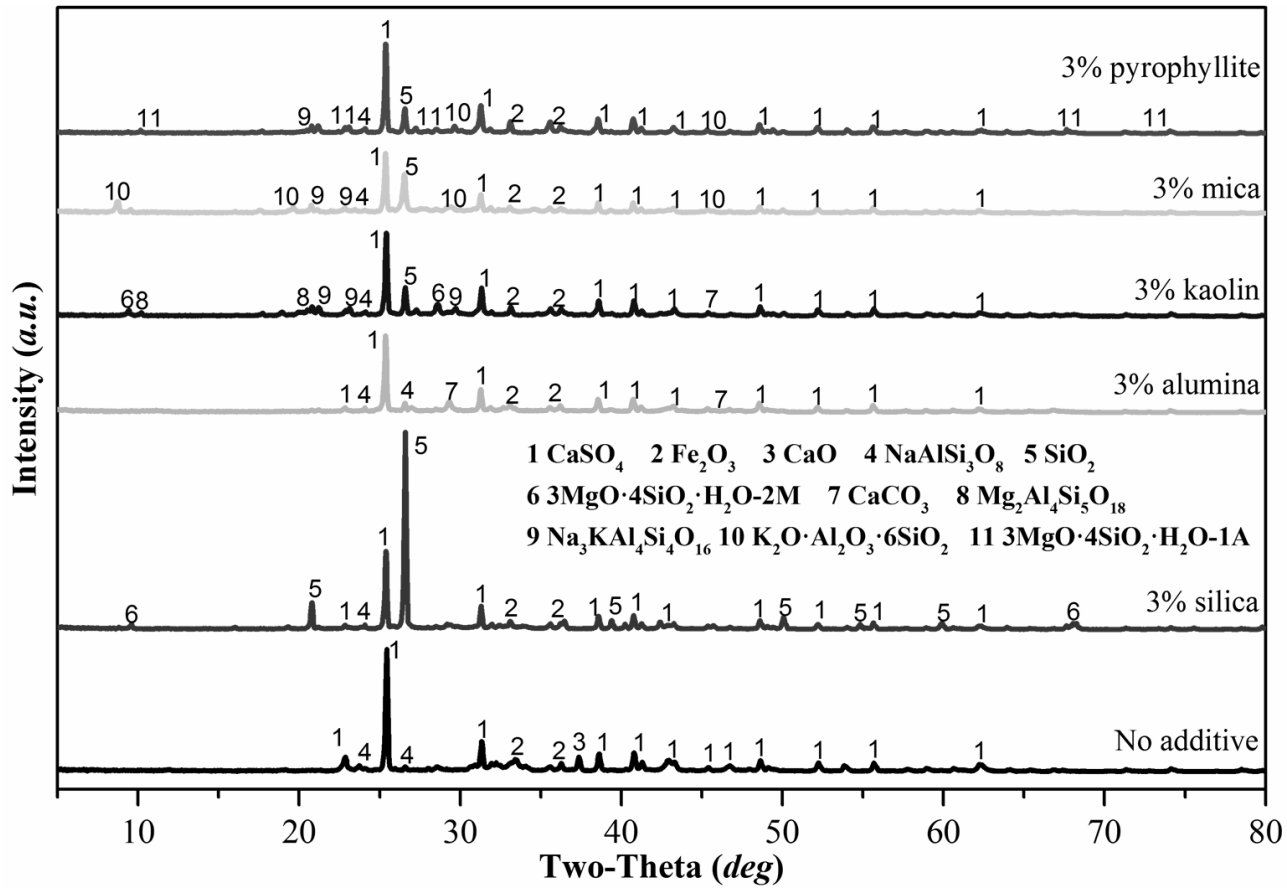

Fig. 5. XRD analysis of the ash samples prepared from Zhundong coal and coal/additive blends.

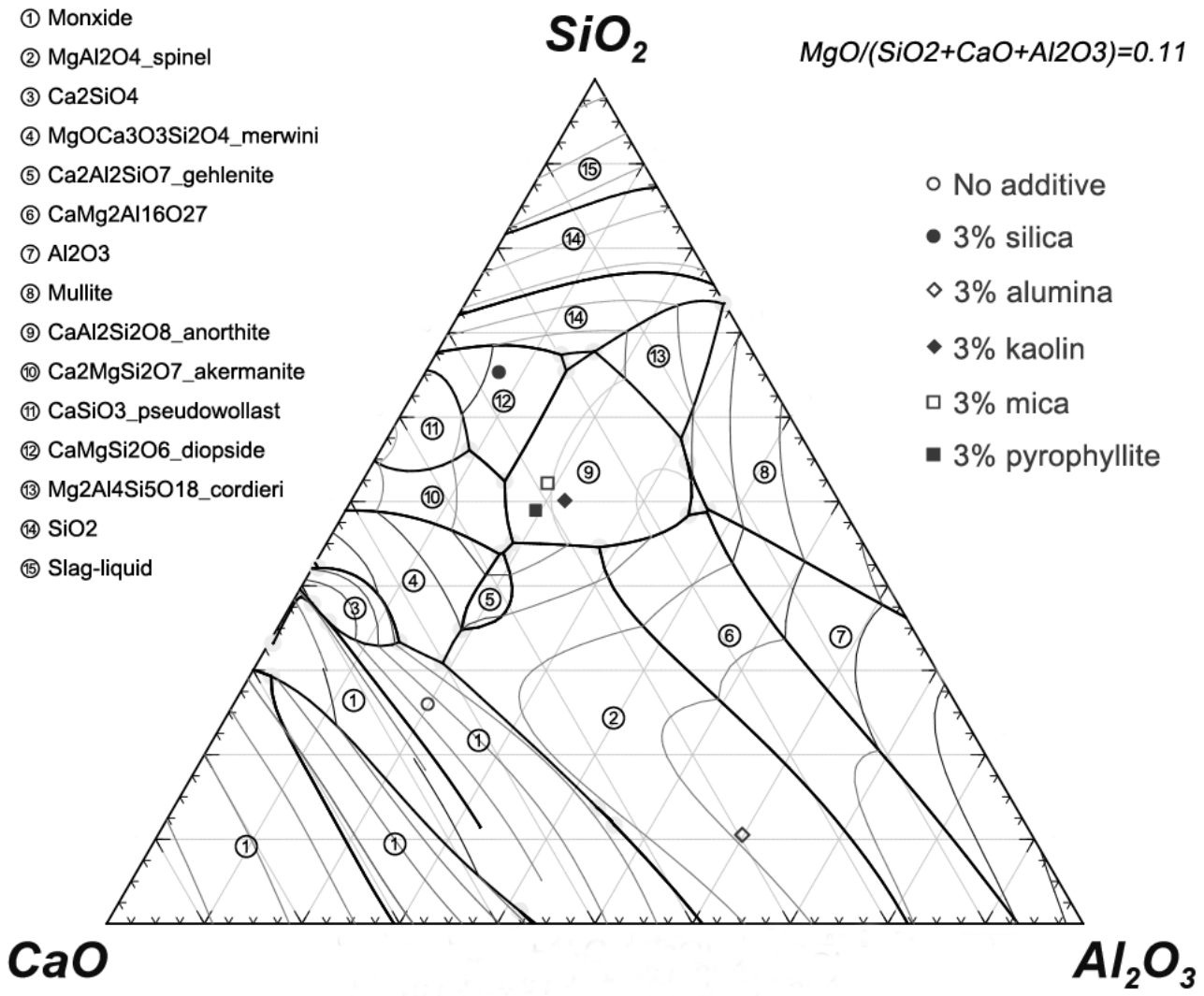

Fig. 6. SiO_2-CaO-MgO-Al_2O_3 ternary phase diagram predicted by FactSage simulations.

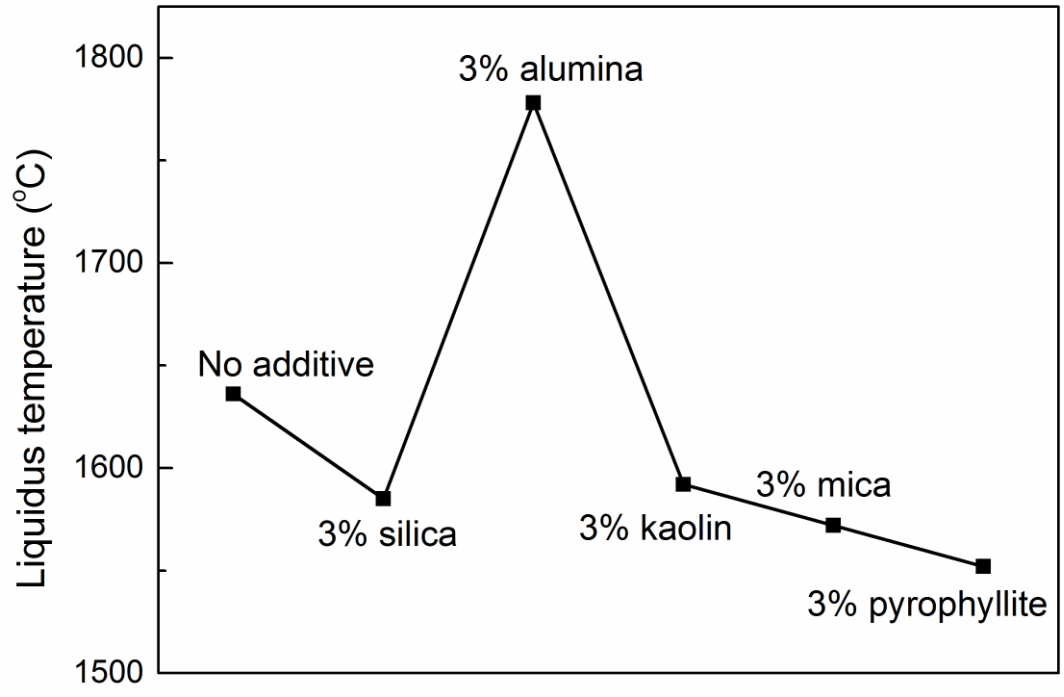

Fig. 7. Liquidus temperatures of various ash samples predicted by FactSage simulations.